

Autocrine signal transmission with extracellular ligand degradation

C B Muratov¹, F Posta² and S Y Shvartsman³

¹ Department of Mathematical Sciences, New Jersey Institute of Technology, Newark, NJ 07102, USA

² Department of Biomathematics, David Geffen School of Medicine, UCLA, Los Angeles, CA 90095, USA

³ Department of Chemical Engineering and Lewis Sigler Institute for Integrative Genomics, Princeton University, Princeton, NJ 08544, USA

E-mail: muratov@njit.edu, fposta@ucla.edu and stas@princeton.edu

Received 18 November 2008

Accepted for publication 23 January 2009

Published 20 February 2009

Online at stacks.iop.org/PhysBio/6/016006

Abstract

Traveling waves of cell signaling in epithelial layers orchestrate a number of important processes in developing and adult tissues. These waves can be mediated by positive feedback autocrine loops, a mode of cell signaling where binding of a diffusible extracellular ligand to a cell surface receptor can lead to further ligand release. We formulate and analyze a biophysical model that accounts for ligand-induced ligand release, extracellular ligand diffusion and ligand–receptor interaction. We focus on the case when the main mode for ligand degradation is extracellular and analyze the problem with the sharp threshold positive feedback nonlinearity. We derive expressions that link the speed of propagation and other characteristics of traveling waves to the parameters of the biophysical processes, such as diffusion rates, receptor expression level, etc. Analyzing the derived expressions we found that traveling waves in such systems can exhibit a number of unusual properties, e.g. non-monotonic dependence of the speed of propagation on ligand diffusivity. Our results for the fully developed traveling fronts can be used to analyze wave initiation from localized perturbations, a scenario that frequently arises in the *in vitro* models of epithelial wound healing, and guide future modeling studies of cell communication in epithelial layers.

1. Introduction

The development and maintenance of animal tissues depends on cell communication by diffusible ligands that act through their cognate cell surface receptors to control cell differentiation, migration, division and death [1]. Ligand–receptor binding activates signaling pathways that can stimulate further ligand release in a responding cell. This mode of cell signaling is called an autocrine loop [2]. When combined with ligand diffusion, this type of positive feedback can lead to traveling waves of cell signaling that have been indeed observed in a number of experimental systems. For example, in the developing *Drosophila* trachea, positive feedback autocrine loop in the highly conserved epidermal growth factor receptor (EGFR) system is responsible for the traveling wave of EGFR activation, which is, in turn, essential for spatial coordination of cell alignment and intercalation [3]. Traveling fronts mediated by autocrine loops can also operate

in adult tissues when they respond to wounding. Cells at the edge of the wound have been shown to secrete a mixture of growth factors and smaller molecules, like ATP, that can initiate the tissue-level waves of cell signaling [4–6]. One function of such fronts is to coordinate the collective migration of cells during the early stages of wound closure.

Recently we have begun to formulate and analyze biophysical models of spatially distributed autocrine loops in order to understand the regulation of traveling waves in these systems [7–9]. Our models accounted for ligand-induced ligand release, extracellular ligand diffusion, reversible binding to surface receptors and receptor-mediated ligand degradation. In a number of such problems we have derived analytical results for the profiles and speeds of propagating waves and explored their nontrivial dependence on the parameters of the biophysical problems. Here we focus on the case when the main pathway for ligand degradation is mediated not by cell surface receptors, but by

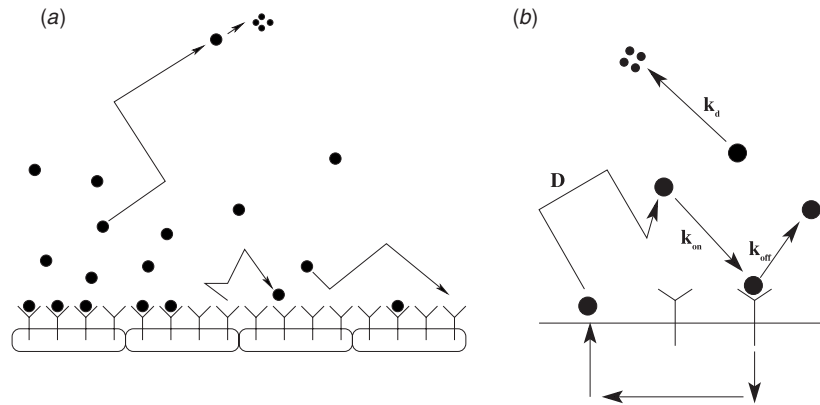


Figure 1. Ligand-mediated signal transmission: the geometry of the system (a) and the elementary processes (b).

the extracellular molecules, such as proteases that can degrade soluble ligands. Based on the combination of analytical and numerical approaches we show that traveling fronts robustly exist in this case, but that their properties can be quite different from those in problems with receptor-mediated ligand degradation.

We begin by considering an idealized epithelium in the form of an extended flat layer of cells bounded by semi-infinite space filled with extracellular matrix. In the following, individual cells are modeled within the continuum approximation. Thus, the system consists of three distinct spatial compartments: the extracellular space where signals can diffuse and undergo reactions with the extracellular medium and its contents, the cell layer where various intracellular processes occur, and the cell layer surface through which signaling molecules are secreted and where they can bind to their specific cell surface receptors. This is illustrated schematically in figure 1.

For simplicity, we will consider signaling mediated by a single signaling molecule (ligand). Ligands are released from the cell surfaces and can diffuse in the extracellular space. The fate of each ligand molecule in the extracellular space is determined by two basic processes. A ligand can bind to its specific cell-surface receptor, causing activation of intracellular signaling cascades which, in turn, can lead to cellular responses affecting further ligand release by cells. Alternatively, a ligand may react with other molecular species present in the extracellular matrix and become incapable of further signaling, either through binding or degradation. In this paper, we make two assumptions regarding the interactions of ligand molecules with their environment. First, we will assume that the cellular response to ligand–receptor binding results in increased secretion of ligands from the surface of the affected cell, generating a positive autocrine feedback loop [10]. Second, we will assume that ligands in the extracellular space are irreversibly inactivated (degraded) via a first-order process.

At the cell surface, the ligand molecule can associate with the cell surface receptor to form a ligand–receptor complex. This complex can then either dissociate to release the ligand molecule back to the extracellular environment, or it can be endocytosed into the cell, where the ligand molecule can be

either reprocessed or destroyed. Endocytosis provides another mechanism of ligand extraction at the cell surface, which may compete with the degradation processes in the bulk of the extracellular medium. Since in this paper we are interested in the role the bulk degradation plays in autocrine signaling, we will simplify our discussion by considering only the extreme case in which endocytosis is negligible in comparison with bulk degradation. This regime accentuates the fact that in the presence of bulk degradation the spatial domains of ligand release and ligand removal are very different, making the problem highly nonlocal.

Mathematically, the processes described in figure 1 may be formulated in terms of the following system of equations:

$$\frac{\partial S}{\partial T} = D \left(\frac{\partial^2 S}{\partial X^2} + \frac{\partial^2 S}{\partial Y^2} + \frac{\partial^2 S}{\partial Z^2} \right) - k_d S, \quad Z > 0, \quad (1)$$

$$D \frac{\partial S}{\partial Z} = \frac{\partial C}{\partial T} - g_s P, \quad Z = 0, \quad (2)$$

$$\frac{\partial C}{\partial T} = k_{on} R S - k_{off} C, \quad Z = 0, \quad (3)$$

$$\frac{\partial P}{\partial T} = -k_p P + g_p \sigma(C/C_T), \quad Z = 0. \quad (4)$$

Here, the variables are as follows: S denotes the concentration of ligand molecules in the extracellular space located at $Z > 0$, where (X, Y, Z) are three-dimensional spatial coordinates; C is the ligand–receptor complex density at the cell surfaces, located at $Z = 0$; P is the density of an intracellular species that mediates the release of ligand molecules into the extracellular space; finally, T is time. Equation (1) describes diffusion of the ligand molecules with diffusion coefficient D and degradation with rate k_d in the extracellular space. Equation (2) provides the boundary condition for the ligand flux at the cell surfaces, which consists of the first term coming from association–dissociation of complexes and the second term describing ligand secretion with rate constant g_s . Equation (3) describes the association–dissociation dynamics of the complexes at the cell surface with binding rate k_{on} , free receptor density R and dissociation rate k_{off} . Lastly, equation (4) describes the response of the intracellular species to the number of ligand–receptor complexes and consists of a first-order degradation process with rate k_p and a production term with rate constant

Table 1. Descriptions and typical values of the model parameters.

Parameter	Description	Typical value
D	Ligand diffusivity	$10^{-6} \text{ cm}^2 \text{ s}^{-1}$
k_{on}	Ligand–receptor binding rate constant	$10^2 \mu\text{M}^{-1} \text{ min}^{-1}$
k_{off}	Ligand–receptor dissociation rate constant	10^{-1} min^{-1}
k_p	Degradation rate constant for the ligand release-mediating intracellular species	10^{-2} min^{-1}
k_d	Ligand degradation constant in the extracellular medium	1 min^{-1}
L	Ligand diffusion length in the extracellular medium	$75 \mu\text{m}$
R	Cell surface receptor density	$10^5/\text{cell}$
C_T	Threshold ligand–receptor complex density	$10^3/\text{cell}$
g_P	Maximum production rate for the ligand release-mediating intracellular species	$10 \text{ min}^{-1}/\text{cell}$
$g_S g_P/k_p$	Maximum ligand secretion rate	$60 \text{ min}^{-1}/\text{cell}$
A	Cell surface area	$25 \mu\text{m}^2$
α	Dimensionless degradation rate	0.01
β	Dimensionless surface capacitance	0.86
s_T	Dimensionless feedback threshold	0.20
v	Dimensionless front speed	0.34

g_P which involves a sigmoidal dependence $\sigma(a)$ on the ratio of the complex density to a threshold value C_T . The latter realizes the mechanism of ligand-induced ligand release responsible for the positive autocrine feedback loop [10]. The model parameters and their typical values are shown in table 1.

Our main results are presented in section 2. Specifically, in section 2.1 we introduce the fast ligand–receptor binding approximation to the full model presented in section 1, in section 2.2 we non-dimensionalize the model and identify the dimensionless parameter groups, in section 2.3 we discuss existence, stability and multiplicity of the steady states supported by the model, in section 2.4 we analyze the traveling front solutions and the dependence of the front speed on the dimensionless model parameters, in section 2.5 we consider a number of limiting regimes of front propagation, and in section 2.6 we perform an analysis of the front speed dependence on the original biophysical parameters. Finally, in section 3 we summarize our findings and further discuss the applicability of our results to time transients and more detailed models of cell signaling.

2. Results

2.1. Fast binding approximation

We now turn to the analysis of the system of equations in (1)–(4). Our first step is to simplify them by assuming that the binding dynamics is very fast. Mathematically, this can be achieved by passing to the limit $k_{\text{on}}, k_{\text{off}} \rightarrow \infty$ with the ratio $k_{\text{on}}/k_{\text{off}}$ fixed. Biophysically, this implies that binding and dissociation are the fastest processes compared to all other processes, i.e., we have $k_{\text{off}} \gg k_p, k_d$. As a result, we can replace equations (2) and (3) with

$$C = \frac{k_{\text{on}}RS}{k_{\text{off}}}, \quad D \frac{\partial S}{\partial Z} = \frac{k_{\text{on}}R}{k_{\text{off}}} \frac{\partial S}{\partial T} - g_S P, \quad Z = 0, \quad (5)$$

where we took into account that both $C \rightarrow (k_{\text{on}}R/k_{\text{off}})S|_{Z=0}$ and $\partial C/\partial T \rightarrow (k_{\text{on}}R/k_{\text{off}})(\partial S/\partial T)|_{Z=0}$ in the limit.

Therefore, when the binding processes are fast, one can assume that the ligand–receptor complex density follows the ligand concentration at the epithelium surface. At the same time, note that the absence of the endocytosis term in equation (3) leads to an appearance of a new capacitance-like term in the effective boundary condition given by equation (5). This is a novel feature of the considered model that was not present in our previous studies of autocrine signaling, in which ligand degradation occurred via ligand-mediated endocytosis [7–9].

2.2. Non-dimensionalization

We now non-dimensionalize the reduced problem given by equations (1), (4) and (5) by introducing the following new variables:

$$t = k_p T, \quad x = \frac{X}{L}, \quad s = \frac{S}{S_0}, \quad p = \frac{P}{P_0}, \quad (6)$$

where

$$L = \sqrt{\frac{D}{k_d}}, \quad S_0 = \frac{g_S g_P}{k_p \sqrt{D k_d}}, \quad P_0 = \frac{g_P}{k_p}, \quad (7)$$

and introducing dimensionless constants

$$\alpha = \frac{k_p}{k_d}, \quad \beta = \frac{k_p k_{\text{on}} R}{k_{\text{off}} \sqrt{D k_d}}, \quad s_T = \frac{C_T k_{\text{off}} k_p \sqrt{D k_d}}{g_S g_P k_{\text{on}} R}. \quad (8)$$

As a result, we obtain the following dimensionless system, which will be the subject of the analysis below:

$$\alpha \frac{\partial s}{\partial t} = \frac{\partial^2 s}{\partial x^2} + \frac{\partial^2 s}{\partial y^2} + \frac{\partial^2 s}{\partial z^2} - s, \quad z > 0, \quad (9)$$

$$\frac{\partial s}{\partial z} = -p + \beta \frac{\partial s}{\partial t}, \quad z = 0, \quad (10)$$

$$\frac{\partial p}{\partial t} = -p + \sigma(s/s_T), \quad z = 0. \quad (11)$$

This model contains three dimensionless parameters: s_T , α and β . The meaning of the first parameter is straightforward,

it represents the degree of excitability of the positive feedback. The parameter α measures the relative speed of degradation (fast degradation compared to intracellular dynamics means $\alpha \ll 1$). The meaning of the parameter β is less straightforward. Roughly speaking, it measures the delay in establishing a steady signaling profile after activation of the positive feedback. Note that the units of time and length were chosen to be the time scale of intracellular reaction k_p^{-1} and the diffusion length $L = (D/k_d)^{1/2}$ of ligands in the extracellular space. Thus, L is the characteristic distance ligand molecules can diffuse away from the cell surfaces before being degraded. On the other hand, observe that in cell signaling problems another combination of the parameters $l = D/(k_{\text{on}}R)$ has the dimension of length and measures the spatial extent of an autocrine loop in the absence of bulk degradation [2]. In terms of these two lengths, we can write $\beta = k_p L / (k_{\text{off}} l)$. From this, one can see that β can be both small and large. The latter does not contradict our assumption $k_p \ll k_{\text{off}}$, however, since it is possible to have $L \gg l$ for sufficiently small values of k_d .

Lastly, the choice of the sigmoidal function σ is dictated by the specifics of the intracellular signaling cascade and the response to its activation, but is typically assumed to be of Hill type in the modeling studies

$$\sigma(a) = \frac{a^\nu}{1 + a^\nu}, \quad (12)$$

with ν sufficiently large [11]. Here, note that the activation threshold s_T is already explicitly contained in the argument of σ in equation (11). In fact, most of our analysis will be performed under a further simplifying assumption of sharp activation threshold, $\nu \rightarrow \infty$, i.e. when the sigmoidal function σ is approximated by

$$\sigma(a) = H(a - 1), \quad (13)$$

where $H(x)$ is the Heaviside step function. We will also make a quantitative comparison between the case $\nu = \infty$ and $\nu < \infty$ for front propagation problems in section 3.

2.3. Steady states and their stability

We begin with the analysis of the steady states of signaling admitted by the model. Under appropriate conditions, one would expect our system to exhibit multistability. Indeed, the cooperativity built into the ligand-mediated ligand release mechanism and the ligand degradation in the bulk represent two competing tendencies with a possibly nontrivial balance. Note, however, that by the non-local nature of the problem all steady states in the system will be spatially inhomogeneous. Therefore, the role of equilibria in the system will be played by the solutions which are constant across the epithelium surface (but not in the normal direction).

Setting $s = s(z)$ in equation (9) and taking into account that the ligand concentration must vanish far from the epithelium, we immediately find that $s(z) = \bar{s} e^{-z}$, where \bar{s} is the ligand concentration at the epithelium surface. Further substituting this expression into equation (4), we find that in an equilibrium $p = \bar{s}$ and \bar{s} needs to satisfy

$$\bar{s} = \sigma(\bar{s}/s_T). \quad (14)$$

This equation always has a trivial solution $\bar{s} = 0$. However, when the value of the threshold s_T becomes sufficiently small, a pair of two new roots of equation (14) appears via a saddle-node bifurcation. When $\nu \rightarrow \infty$ in equation (12), the roots of equation (14) are explicitly

$$\bar{s}_1 = 0, \quad \bar{s}_2 = s_T, \quad \bar{s}_3 = 1, \quad (15)$$

when $s_T < 1$. Furthermore, it is not difficult to see in this case that $\bar{s} = 0$ and $\bar{s} = 1$ are stable equilibria, while $\bar{s} = s_T$ is unstable. The stability of $\bar{s} = 0$ and $\bar{s} = 1$ equilibria should be already clear from physical considerations, since when \bar{s} is sufficiently close to those values, equations (1) and (4) effectively decouple. The analysis, however, is rather involved because the nonlocality of the problem introduces memory effects. In appendix A we explicitly demonstrate stability of these equilibria with respect to perturbations in p of the form $\delta p = \text{Re}(a_0 e^{-iqx})$. We also note that the analysis of appendix A can be straightforwardly extended to the general case of $\nu < \infty$ and small initial perturbations of general form, the results are expected to be unchanged.

Finally, let us note that in the original, unscaled variables the condition $s_T < 1$ of bistability for sharp threshold nonlinearity can be rewritten as

$$c_T < \frac{k_{\text{on}}R}{\sqrt{Dk_d}}, \quad c_T = \frac{k_{\text{off}}k_p}{g_s g_P} C_T. \quad (16)$$

Here we introduced a dimensionless parameter c_T , which is simply the threshold C_T rescaled by the value of C at which the maximum secretion flux and the dissociation flux are equal. Thus, the condition of bistability states that the rescaled threshold c_T must be smaller than the ratio of two quantities, with the dimension of velocity, characterizing binding and degradation.

2.4. Traveling fronts

A common dynamical feature of the considered class of reaction-diffusion systems is the phenomenon of front propagation [12–17]. In particular, propagation of fronts of signaling activity has been observed in a number of cell communication models in which reaction and diffusion occur in spatially separated compartments [7, 9, 18]. To see whether front propagation is still possible in autocrine systems in the presence of bulk degradation, we constructed exact traveling wave solutions in the form of planar fronts of signaling activity, when the nonlinearity σ is of sharp threshold type, i.e. given by equation (13).

Without a loss of generality, we may assume that the front solution is independent of the y -variable. Thus, we look for solutions of equations (9)–(11) in the form $s = s(x - vt, z)$ and $p = p(x - vt)$. Substituting this ansatz into equations (9)–(11), we obtain the following boundary-value problem for the front profile:

$$\frac{\partial^2 s}{\partial x^2} + \frac{\partial^2 s}{\partial z^2} + \alpha v \frac{\partial s}{\partial x} - s = 0, \quad z > 0 \quad (17)$$

$$\frac{\partial s}{\partial z} + p + \beta v \frac{\partial s}{\partial x} = 0, \quad z = 0, \quad (18)$$

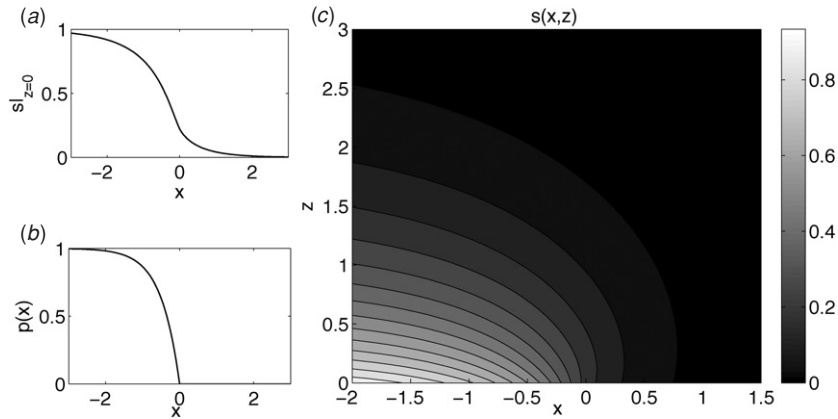


Figure 2. The profile of the traveling front at $\alpha = 0.5$, $\beta = 1$ and $s_T = 0.2226$.

$$v \frac{\partial p}{\partial x} - p + H(s - s_T) = 0, \quad z = 0. \quad (19)$$

By fronts we mean those solutions of equations (17)–(19) for which the level of signaling (which is an increasing function of s at $z = 0$) is monotone in x . Without a loss of generality we may assume that in a front $\partial s(x, 0)/\partial x < 0$, with the profile approaching zero at $x = +\infty$ and the state of high signaling at $x = -\infty$:

$$p(+\infty) = 0, \quad s(+\infty, z) = 0, \quad (20)$$

$$p(-\infty) = 1, \quad s(-\infty, z) = e^{-z}. \quad (21)$$

It is easy to see from equation (19) that a monotonic decrease of $s(x, 0)$ implies that $p(x)$ is non-increasing. On the other hand, any bounded solution $s(x, z)$ of equations (17), (18), (20) and (21) with non-increasing and bounded $p(x)$ is, in fact, strictly monotonically decreasing in x for each $z \geq 0$. The latter follows from an application of the maximum principle techniques to the boundary-value problem in equations (17), (18), (20) and (21), we outline the argument in appendix B. Note that the last statement also provides a consistency verification of the monotonicity assumption for $s(x, 0)$.

By strict monotonicity of $s(x, 0)$, there exists a unique point $x = x_0$ at which the threshold of the feedback loop activation is crossed, provided that $0 < s_T < 1$. By translational symmetry we may assume that this happens at the origin, i.e. we have $s(0, 0) = s_T$. Also, we can consider the case $v > 0$ only, i.e., when the on-state of signaling invades the off-state from left to right, since the problem is invariant with respect to the transformation

$$x \rightarrow -x, \quad z \rightarrow z, \quad v \rightarrow -v, \quad (22)$$

$$s_T \rightarrow 1 - s_T, \quad p \rightarrow 1 - p, \quad s \rightarrow e^{-z} - s. \quad (23)$$

Therefore, if the solution with $v > 0$ is found, then another solution with $v < 0$ can be obtained from the first one via the transformation above. In particular, if $s_T = s_T^+(v)$ is the threshold at which the front propagates with speed $v > 0$, then $s_T = s_T^-(v)$, where

$$s_T^-(v) = 1 - s_T^+(-v), \quad (24)$$

is the threshold at which the front moves with speed $v < 0$, i.e. when the off-state invades the on-state from right to left. In particular, this implies that $v = 0$ must occur at $s_T = \frac{1}{2}$.

We solved the boundary-value problem in equations (17)–(19), using Fourier transform techniques (the details are presented in appendix C). The typical solution profile for a particular set of parameters is presented in figure 2. One can see that in agreement with the general discussion above, the solution has a monotone signaling profile, and the distribution of s in the extracellular medium is tightly localized next to the epithelium surface and advancing into the region with low signaling activity. The speed of the front is given by the implicit relation $s_T = s_T^+(v)$ (for $v > 0$), where

$$s_T^+(v) = \frac{1}{\pi} \int_{\frac{1}{2}(\alpha v + \sqrt{4 + \alpha^2 v^2})}^{\infty} \left(\frac{\sqrt{\tau^2 - \alpha v \tau - 1}}{\tau(1 + v\tau)((1 + \beta^2 v^2)\tau^2 - \alpha v \tau - 1)} \right) d\tau. \quad (25)$$

In particular, uniqueness of solutions (up to translations) follows from $s_T^+(0) = \frac{1}{2}$, $\lim_{v \rightarrow \infty} s_T^+(v) = 0$, and strict monotonic decrease of the function $s_T^+(v)$ in equation (25) for all $v > 0$, demonstrated at the end of appendix C. To summarize:

for every $0 < s_T < 1$, there exists a unique speed $v = v(\alpha, \beta, s_T)$ and a unique, up to translations, traveling front profile for each $\alpha > 0$ and $\beta > 0$.

The values of the dimensionless parameters and the front speed corresponding to the typical set of dimensional model parameters in table 1 are listed at the bottom of that table. The graph of the threshold s_T as a function of the front speed v for the same values of α and β as in figure 2 is shown in figure 3.

2.5. Asymptotic regimes

We used equation (25) to study parametric dependence of the dimensional front propagation speed

$$V = Lk_p v(\alpha, \beta, s_T), \quad (26)$$

on various model parameters of the problem. Note that for fixed v the value of s_T from equation (25) is a monotonically

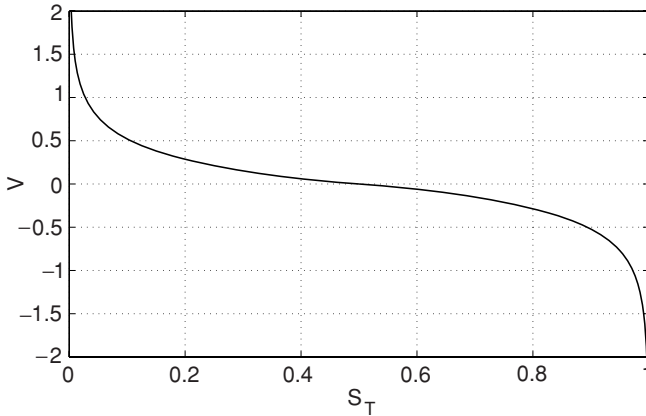


Figure 3. Dependence of v on s_T for $\alpha = 0.5$ and $\beta = 1$ obtained from equation (25).

decreasing function of both α and β (see the end of appendix C). Nevertheless, since most of the dimensional model parameters enter into these dimensionless quantities in non-trivial combinations, it is not obvious what to expect for the dependence of the dimensional front speed on, e.g., the diffusion coefficient D or the degradation constant k_d . To get a better understanding of the dependence of the dimensional front speed on the model parameters, we first undertook a study of a number of asymptotic parameter regimes (for the derivation of the corresponding reduced models, see appendix D). We start with the case in which both parameters α and β are small. This case corresponds to the limit in which the bulk degradation is very fast and, therefore, can be treated under the quasi steady-state approximation. The smallness of β , in turn, implies that the capacity of the epithelium surface is negligible, and so upon secretion ligands quickly diffuse far from the cell surface. In this situation the time scale of the problem is determined by the dynamics of the intracellular species.

It is easy to pass to the limit $\alpha \rightarrow 0$ and $\beta \rightarrow 0$ in equation (25), since the integrand and the lower limit of integration depend continuously on these parameters. As a result, we get explicitly

$$s_T^+(v) \simeq \frac{1}{\pi} \int_1^\infty \frac{d\tau}{\tau(1+v\tau)\sqrt{\tau^2-1}} = \frac{1}{2} - \frac{v \sec^{-1}(v)}{\pi\sqrt{v^2-1}}. \quad (27)$$

In particular, we obtain

$$s_T^+(v) \simeq \frac{1}{\pi v}, \quad v \gg 1, \quad (28)$$

$$s_T^+(v) \simeq \frac{1}{2} - \frac{v}{\pi} \ln\left(\frac{2}{v}\right), \quad v \ll 1. \quad (29)$$

From the first equation above, the dimensional front speed V for $s_T \ll 1$ can be approximated as

$$V \simeq \frac{gsg_p k_{on} R}{\pi k_{off} k_d C_T} = \left(\frac{k_p}{k_d}\right) \frac{k_{on} R}{\pi c_T}, \quad (30)$$

where c_T is given in equation (16). This result appears to be quite surprising, since it turns out that the front propagation speed is independent of both the ligand diffusion constant D

and the intracellular degradation constant k_p in this regime. On the other hand, the speed depends strongly on the binding-dissociation kinetics, as well as on the degradation rate.

Now let us consider the case $\alpha \gg 1$ and $\beta \ll \alpha$ in which ligand degradation in the bulk is slow compared to other processes. In this case, we can neglect the delay in the response of the intracellular species to signaling, as well as the cell surface capacity. Setting $\beta = 0$ and treating v to be of order $\alpha^{-1} \ll 1$, in the limit of $\alpha \rightarrow \infty$ we obtain

$$\begin{aligned} s_T^+(v) &\simeq \frac{1}{\pi} \int_{\frac{1}{2}(\alpha v + \sqrt{4 + \alpha^2 v^2})}^\infty \frac{d\tau}{\tau \sqrt{\tau^2 - \alpha v \tau - 1}} \\ &= \frac{1}{\pi} \cos^{-1} \left(\frac{\alpha v}{\sqrt{4 + \alpha^2 v^2}} \right). \end{aligned} \quad (31)$$

In particular, we have

$$s_T^+(v) \simeq \frac{2}{\pi \alpha v}, \quad \alpha v \gg 1, \quad (32)$$

$$s_T^+(v) \simeq \frac{1}{2} - \frac{\alpha v}{2\pi}, \quad \alpha v \ll 1. \quad (33)$$

Actually, in this case the front speed may be explicitly expressed in terms of the threshold. After some simple algebra, we find that

$$v \simeq \frac{2}{\alpha \tan(\pi s_T)}. \quad (34)$$

Writing the dimensional front speed V for $s_T \ll 1$, from (32) we obtain the following approximate expression:

$$V \simeq \frac{2gsg_p k_{on} R}{\pi k_{off} k_p C_T} = \frac{2k_{on} R}{\pi c_T}. \quad (35)$$

One can see that now the speed does not depend on the ligand diffusion constant D and the degradation constant k_d . Note that in the related models of intracellular calcium signaling the independence of the front speed from the diffusion constant was already pointed out in [18]. On the other hand, the front speed strongly depends on k_p , in addition to the details of association-dissociation kinetics. Note that since typically $k_{off} \gg k_p$, the front speed will be greater in this regime for the same value of c_T , compared to the case of $\alpha \ll 1$ and $\beta \ll 1$ analyzed earlier.

Finally, the third case of interest, $\beta \gg 1$ and $\alpha \ll \beta$ corresponds to fast bulk degradation and large cell surface capacitance. Setting $\alpha = 0$ and treating now v as a quantity of order $\beta^{-1} \ll 1$, in the limit $\beta \rightarrow \infty$ we obtain

$$\begin{aligned} s_T^+(v) &\simeq \frac{1}{\pi} \int_1^\infty \frac{\sqrt{\tau^2-1}}{\tau((1+\beta^2 v^2)\tau^2-1)} d\tau \\ &= \frac{1}{2} \left(1 - \frac{\beta v}{\sqrt{1+\beta^2 v^2}} \right). \end{aligned} \quad (36)$$

In particular, for large and small values of βv we have the following expansions:

$$s_T^+(v) \simeq \frac{1}{4\beta^2 v^2}, \quad \beta v \gg 1, \quad (37)$$

$$s_T^+(v) \simeq \frac{1}{2} - \frac{\beta v}{2}, \quad \beta v \ll 1. \quad (38)$$

Also, as in the previous case, we can explicitly express the front speed in terms of the threshold. After a little algebra we arrive at the following expression:

$$v = \frac{1 - 2s_T}{2\beta\sqrt{s_T(1 - s_T)}}. \quad (39)$$

The dimensional front speed V for $s_T \ll 1$, in turn, is given by the following approximate expression:

$$V \simeq \left(\frac{D^3 g_S^2 g_P^2 k_{\text{off}}^2}{16k_d k_{\text{on}}^2 R^2 k_p^2 C_T^2} \right)^{1/4} = \frac{k_{\text{off}}(lL)^{1/2}}{2C_T^{1/2}}, \quad (40)$$

where $l = D/(k_{\text{on}}R)$ is the range of the autocrine loop [2].

2.6. Parametric analysis

We now turn to the study of the dependence of the dimensional front speed V on the dimensional model parameters. In all cases, we will only consider the situation in which the signal propagates with positive speed, i.e. when $s_T < \frac{1}{2}$, so that the state of high signaling is invading the no-signaling state. Let us start from the dependence of V on the feedback threshold C_T . Clearly, since C_T only enters the dimensionless problem via the value of s_T , an increase in C_T will result in a decrease of the front speed. This behavior is, of course, quite expected. Similarly, the front speed is an increasing function of g_S and g_P .

One would also expect that the dimensional front speed V is a decreasing function of k_d . This, however, already cannot be seen so straightforwardly from equation (25), since, as k_d increases, the value of s_T increases, but at the same time the values of α and β decrease. Also, the value of L is decreasing with k_d . Nevertheless, we found numerically for a wide range of the parameters that V decreases as k_d increases. In particular, when the threshold C_T of the feedback is sufficiently small, an increase in k_d pushes the parameters into the regime where $\alpha \ll 1$ and $\beta \ll 1$, hence V is given by equation (30). From that equation one can explicitly see that V is a decreasing function of k_d . On the other hand, when k_d tends to zero, we have $\alpha \gg \beta \gg 1$. In this limit V is given by equation (35) and, in fact, becomes essentially independent of k_d for sufficiently small k_d .

Let us now analyze the dependence of V on k_p . When the value of k_p is decreased, α , β and s_T all decrease. Therefore, for small enough values of k_p the front speed can be approximated by equation (30), which states that V is essentially independent of k_p in this regime. On the other hand, increasing k_p results in an increase of s_T , with V becoming zero at a critical value of k_p . Therefore, V is expected to decrease when the value of k_p is increased.

As far as the dependence on the binding dissociation is concerned, one can see that the corresponding rate constants enter V only via the combination $k_{\text{on}}R/k_{\text{off}}$. Therefore, without a loss of generality we can study the effect of changing those parameters by considering V as a function of, say, the receptor density R . A change of R by a factor of λ results in the dimensional front velocity change by a factor of

$$V_\lambda/V = v(\alpha, \lambda\beta, \lambda^{-1}s_T)/v(\alpha, \beta, s_T). \quad (41)$$

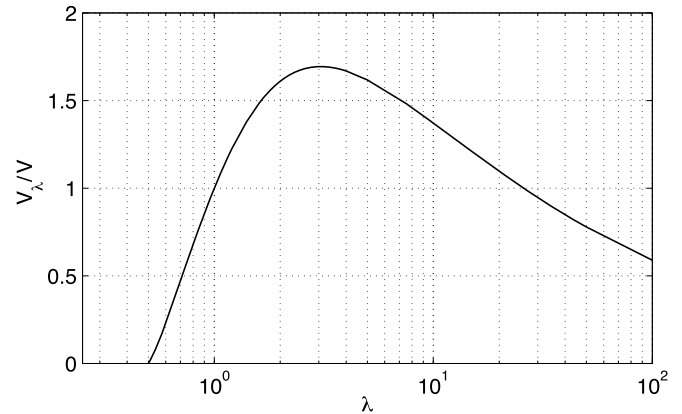


Figure 4. Dependence of V_λ/V on λ obtained from equation (41) for $\alpha = 0.75$, $\beta = 0.5$, $s_T = 0.25$.

From this one can make two observations. First, at a certain critical value of λ we will have $V_\lambda = 0$. On the other hand, for λ sufficiently large we have $\beta_\lambda = \lambda\beta \gg 1$ and $s_T^\lambda = \lambda^{-1}s_T \ll 1$, hence from equation (40) we can see that $V_\lambda/V \sim \lambda^{-1/2} \rightarrow 0$ as $\lambda \rightarrow \infty$. This implies that V_λ must have a maximum for some value of λ . We verified this to be the case, figure 4 shows the dependence of V_λ on λ for a particular set of parameters. Let us point out the similarity of this phenomenon to that observed by us earlier in the studies of a similar model [7]. Note, however, that in [7] the maximum propagation speed was observed only in systems in which the ligand was allowed to diffuse in an extracellular medium layer of finite thickness. The maximum of V in [7] was absent in semi-infinite media, as opposed to the results presented here.

Perhaps the most surprising behavior of the dimensional front speed V is exhibited by its non-monotone dependence on the ligand diffusion coefficient D . If D is changed by a factor of μ , the front speed will change by a factor of

$$V_\mu/V = \mu^{1/2}v(\alpha, \mu^{-1/2}\beta, \mu^{1/2}s_T)/v(\alpha, \beta, s_T). \quad (42)$$

Once again, at certain critical value of μ we have $V_\mu = 0$. On the other hand, when the value of μ is decreased, we have $\beta_\mu = \mu^{-1/2}\beta \gg 1$ and $s_T^\mu = \mu^{1/2}s_T \ll 1$. Therefore, by equation (40) we must have $V_\mu/V \sim \mu^{3/4} \rightarrow 0$ as $\mu \rightarrow 0$, and as in the case of the R -dependence, the front speed V has a maximum at a certain value of the diffusion coefficient D . Figure 5 shows this to be the case for a particular set of parameters. Physically, this can be explained by an interplay between the transport and degradation, which determines whether the amount of secreted ligands is sufficient to activate the feedback. Note that the observed non-monotone dependence of the front velocity on the diffusion coefficient goes even further than the anomalous scalings reported earlier in the studies of waves of calcium signaling [18].

3. Discussion

To summarize, we have analyzed ligand-mediated signal transmission in a mechanistic model of an autocrine system where ligand degradation occurs in the extracellular medium. We have shown that long-range signal transmission by

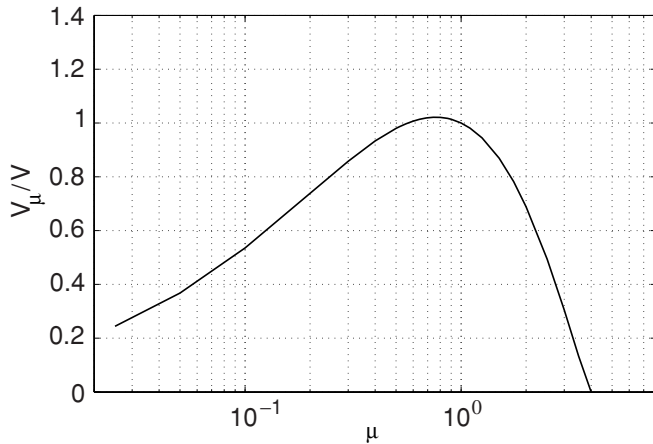


Figure 5. Dependence of V_μ/V on μ obtained from equation (42) for $\alpha = 0.75$, $\beta = 0.5$, $s_T = 0.25$.

means of self-sustained traveling fronts is possible in such systems. Autocrine waves in systems with extracellular ligand degradation have a number of unusual features in comparison with the waves in systems with receptor-mediated ligand degradation. The most striking feature of these waves which is revealed by our analysis is the non-monotonic dependence of their speed on the ligand diffusion constant. The analysis of the original nonlinear and nonlocal problem presents a number of challenges. One of them is related to different spatial dimensionality of the domains for ligand diffusion and processing. Specifically, three-dimensional diffusion of the ligand is coupled with two-dimensional front of intracellular signaling in the cellular layer. This coupling becomes especially non-trivial, since ligand concentration level is determined by the ligand degradation in the three-dimensional extracellular space, while ligand production is due to secretion through the two-dimensional surface of the epithelial layer.

Focusing on the analytically tractable case of infinitely sharp nonlinearity in the ligand-induced ligand release feedback loop, we were able to obtain exact expressions that link the speed of propagation and other wave characteristics to the parameters of the biophysical processes, such as diffusion rates, receptor expression level, etc. At the same time, the implicit nature of the derived equations required more detailed

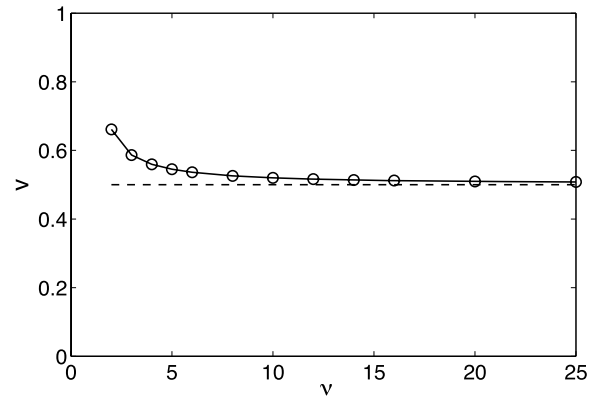


Figure 7. Comparison of the front speed for the Hill nonlinearity with that of the sharp threshold nonlinearity for simulation in figure 6.

analysis of parametric dependences which was guided by a number of limiting cases identified by us. Our results for the fully developed traveling fronts can be used to analyze wave initiation from localized perturbations, a scenario that frequently arises *in vitro* and during epithelial wound healing.

To corroborate this scenario in our model, we performed numerical simulations of the time-dependent problem described by equations (9)–(11). In order to simulate the boundary-value problem, we adapted the method of geometric optimal grids [19] to the problem under consideration (see appendix E for details). Also, a sufficiently large but finite value of the Hill coefficient ν was used. As expected [12, 13, 17], when $s_T < 1/2$ the system exhibits threshold-like behavior when exposed to localized perturbations. Depending on the size of the initial stimulus, the system either remains in the no-signaling state or switches to the state of high signaling. The result of one such simulation for $\alpha = 1$, $\beta = 0.5$, $s_T = 0.1327$ and $\nu = 8$, using a geometric optimal grid code with the in-plane step $h_\perp = 0.1$ and $n = 8$, is shown in figure 6. As can be seen from this figure, switching occurs by a front propagating from the location of the stimulus to the region of no signaling.

Finally, let us note that our results derived for the case of the sharp threshold nonlinearity in the feedback loop are an asymptotic limit of the more general case of the Hill nonlinearity. In practice, however, they give a very good

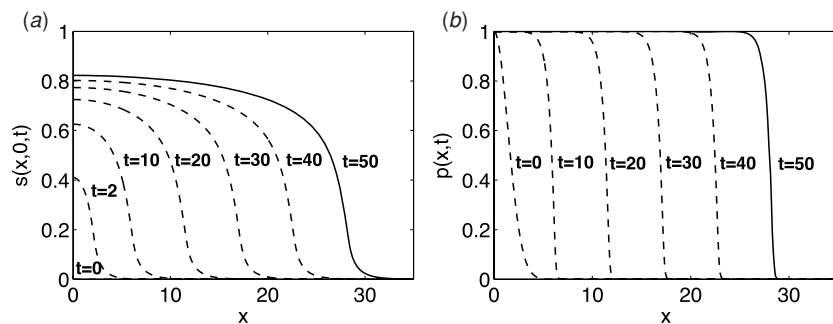


Figure 6. A transient response to a localized stimulus in p obtained by solving equations (9)–(12) with no-flux boundary conditions at $x = 0$ and $x = 50$, and $\alpha = 1$, $\beta = 0.5$, $\nu = 8$, and $s_T = 0.1327$. The initial conditions are $s = 0$, $p = e^{-x^2/4}$.

approximation for the case of finite values of ν . In particular, we found numerically that traveling fronts persist in the case $\nu < \infty$, and that the front speed is quantitatively captured by the analysis of section 2.4. Figure 7 shows the deviation of the front speed obtained numerically for the same parameters as in figure 6 from that of the prediction of equation (25) for different values of ν . One can see that the agreement is within 10% already for $\nu \geq 5$.

Acknowledgments

The authors gratefully acknowledge valuable discussions with P Gordon. This work was supported, in part, by NIH via grants R01 GM076690 and K25AI41935 (FP), and by NSF via grants DMS-0718027 (CBM), DMS-0349195 (FP) and DMS-0718604 (SYS).

Appendix A. Stability of equilibria

Consider (9)–(11), with σ given by (13), and let us perturb, say, the equilibrium $\bar{s} = p = 1$ by $\delta p = \text{Re}(a_0 e^{-iqx})$. Let us look for the solution in the form

$$p = 1 + \text{Re}\{a(t) e^{-iqx}\}, \quad s = e^{-z} + \text{Re}\{b(t, z) e^{-iqx}\}, \quad (\text{A.1})$$

with $a(0) = a_0$ and $b(0, z) = 0$. Assuming that $s > s_T$ for all time (which is expected to be true at least for sufficiently small a_0 in case of stability), we can write the following equations for a and b :

$$a_t = -a + a_0 \delta(t), \quad (\text{A.2})$$

$$\alpha b_t = b_{zz} - (1 + q^2)b, \quad (\text{A.3})$$

$$b_z = -a + \beta b_t, \quad (\text{A.4})$$

where $\delta(t)$ denotes the Dirac delta-function. Further applying Fourier transform

$$\hat{a}_\omega = \int_{-\infty}^{+\infty} a(t) e^{i\omega t} dt, \quad \hat{b}_\omega(z) = \int_{-\infty}^{+\infty} b(t, z) e^{i\omega t} dt, \quad (\text{A.5})$$

to a and b and solving (A.3) with an extra condition that the solution vanishes when $z \rightarrow \infty$, we find that

$$\hat{b}_\omega(z) = \hat{b}_\omega(0) \exp(-z\sqrt{1+q^2-i\alpha\omega}), \quad (\text{A.6})$$

where the branch cut in the definition of the square root is chosen along the imaginary axis from $\omega = -i\infty$ to $\omega = -i(1+q^2)/\alpha$.

Solving (A.2) and substituting this solution into (A.4) together with (A.6) we find

$$\hat{a}_\omega = \frac{a_0}{1-i\omega}, \quad (\text{A.7})$$

$$\hat{b}_\omega = \frac{a_0 \exp(-z\sqrt{1+q^2-i\alpha\omega})}{(1-i\omega)(\sqrt{1+q^2-i\alpha\omega}-i\beta\omega)}. \quad (\text{A.8})$$

Finally, inverting the Fourier transform, we obtain

$$a(t) = a_0 e^{-t}, \quad b(t, z) = \frac{a_0}{2\pi} \int_{-\infty}^{+\infty} e^{-i\omega t} g(\omega, z) d\omega, \quad (\text{A.9})$$

where

$$g(\omega, z) = \frac{e^{-z\sqrt{1+q^2-i\alpha\omega}}}{(1-i\omega)(\sqrt{1+q^2-i\alpha\omega}-i\beta\omega)}. \quad (\text{A.10})$$

The first equation in (A.9) is, of course, expected, because the dynamics of p decouples from that of s when $s > s_T$, and, in particular, we have $a \rightarrow 0$ exponentially as $t \rightarrow \infty$. The second equation is more complicated. However, as is well-known, since for $t \gg 1$ the integral in the second equation of (A.9) contains a rapidly oscillating term, we must have $b(t, z) \rightarrow 0$ as $t \rightarrow \infty$ for all z , hence, stability (more precisely, the result follows by Riemann–Lebesgue lemma, since $g(\cdot, z) \in L^1(\mathbb{R})$ for each $z \geq 0$). A more detailed analysis of the integral shows that convergence is, in fact, exponential (we do not present this rather tedious analysis here).

Finally, to show instability of the $\bar{s} = p = s_T$ equilibrium, we perturb p uniformly by $\delta p = a_0 > 0$ and look for the solution in the form

$$p = s_T + \text{Re}\{a(t)\}, \quad s = s_T e^{-z} + \text{Re}\{b(t, z)\}, \quad (\text{A.11})$$

with $a(0) = a_0$ and $b(0, z) = 0$. Retracing the line of arguments above, after some rather lengthy algebra we obtain

$$b(t, 0) = \int_0^t g(t-\tau)a(\tau) d\tau, \quad (\text{A.12})$$

where $a(t) = 1 - s_T + (a_0 + s_T - 1)e^{-t}$ and

$$g(t) = \frac{2\beta\lambda_+ e^{-\lambda_+ t}}{\sqrt{\alpha^2 + 4\beta^2}} + \frac{1}{\pi} \int_{\alpha^{-1}}^{+\infty} \frac{\sqrt{\alpha\lambda - 1}}{\beta^2\lambda^2 + \alpha\lambda - 1} e^{-\lambda t} d\lambda, \quad (\text{A.13})$$

with

$$\lambda_+ = \frac{-\alpha + \sqrt{\alpha^2 + 4\beta^2}}{2\beta^2}. \quad (\text{A.14})$$

From these formulae one can see that $g(t) > 0$, and so both $a(t) > 0$ and $b(t, 0) > 0$, justifying the assumptions used to derive these formulae. Therefore, in view of $\int_0^\infty g(t) dt = 1$, we have $p(t), \bar{s}(t) \rightarrow 1$ as $t \rightarrow \infty$.

Appendix B. Monotonicity of the ligand profile

To show that monotonicity of $p(x)$ implies that of $s(x, z)$ for each z is a rather straightforward exercise in the application of the strong maximum principle for elliptic boundary-value problems [20]. Here for simplicity we outline the proof of this statement under the assumption that p is a strictly monotonically decreasing function, i.e. $dp/dx < 0$ for all x . A slightly more technical proof still works in the case $dp/dx \leq 0$, yielding strict monotonicity of s in x as well.

It is clear that by linearity the function $u = -\partial s/\partial x$ solves the same kind of boundary-value problem as s

$$\frac{\partial^2 u}{\partial x^2} + \frac{\partial^2 u}{\partial z^2} + \alpha v \frac{\partial u}{\partial x} - u = 0, \quad z > 0 \quad (\text{B.1})$$

$$\frac{\partial u}{\partial z} + g + \beta v \frac{\partial u}{\partial x} = 0, \quad z = 0, \quad (\text{B.2})$$

where $g = -\partial p/\partial x > 0$. Under the assumption that the boundary conditions for s at $z = \pm\infty$ hold uniformly in $C^1([0, +\infty))$, we have $u(x, z) \rightarrow 0$ uniformly in z as $x \rightarrow \pm\infty$. Furthermore, by standard regularity theory u is uniformly bounded when $z \geq 1$ for any bounded solution of (17) and, therefore, decays uniformly to zero as $z \rightarrow \infty$, in view of the fact that $\bar{u} = C e^{-z}$ with C large enough is a supersolution for (B.1) in $\{z \geq 1\}$ [20].

We want to show that, in fact, $u(x, z) > 0$ for all $-\infty < x < +\infty$ and $0 \leq z < +\infty$. So, suppose first that $u < 0$ somewhere. In view of the uniform decay of u at infinity, the function u must attain its minimum at some point (x_0, z_0) , with $-\infty < x_0 < +\infty$ and $0 \leq z_0 < +\infty$, and by our assumption $u(x_0, z_0) < 0$. Since this is a minimum of u , we must have $\partial u/\partial x = 0$ at that point. If $z_0 > 0$, then from (B.1) we have

$$0 \leq \left(\frac{\partial^2 u}{\partial x^2} + \frac{\partial^2 u}{\partial z^2} \right) \Big|_{(x_0, z_0)} = u(x_0, z_0). \tag{B.3}$$

But the latter is impossible, since the right-hand side of this expression is strictly negative. If, on the other hand, $z_0 = 0$, then by (B.2) we get

$$\frac{\partial u}{\partial z} \Big|_{(x_0, z_0)} = -g(x_0) < 0, \tag{B.4}$$

which, once again contradicts the fact that (x_0, z_0) is a minimum of u . Thus, $u \geq 0$ and, by strong maximum principle this implies $u > 0$ for all $z > 0$ [20]. In fact, we have $u > 0$ for $z = 0$ as well, since otherwise the point where $u = 0$ at $z = 0$ is a minimum, which contradicts (B.4)

Appendix C. Construction of the exact traveling front solution

Assuming that $s(x, 0)$ is a strictly monotonically decreasing function of x and that the threshold $s = s_T$ is crossed at $x = 0$, we can rewrite (17)–(19) as follows:

$$\frac{\partial^2 s}{\partial x^2} + \frac{\partial^2 s}{\partial z^2} + \alpha v \frac{\partial s}{\partial x} - s = 0, \quad z > 0 \tag{C.1}$$

$$\frac{\partial s}{\partial z} + p + \beta v \frac{\partial s}{\partial x} = 0, \quad z = 0, \tag{C.2}$$

$$v \frac{\partial p}{\partial x} - p + H(-x) = 0, \quad s(0, 0) = s_T. \tag{C.3}$$

Introducing the Fourier transform in the x -direction

$$\hat{s}_q(z) = \int_{-\infty}^{+\infty} e^{-iqx} s(x, z) dx, \quad \hat{p}_q = \int_{-\infty}^{+\infty} e^{-iqx} p(x) dx. \tag{C.4}$$

and computing the bounded solution of (17), (19) in Fourier space, we obtain

$$\hat{s}_q(z) = \hat{s}_q(0) e^{-z\sqrt{1+q^2-i\alpha vq}}, \quad \hat{p}_q = \frac{i}{(q+i0)(1-ivq)}. \tag{C.5}$$

Here we chose the analytic branch of the square root that has a positive real part and noted that the pole at the origin in the expression for \hat{p}_q should lie below the real axis.

Using the solution just obtained, we can compute

$$\hat{s}'_q(0) = -\sqrt{1+q^2-i\alpha vq} \hat{s}_q(0). \tag{C.6}$$

This, in turn, can be substituted into the Fourier transform of the boundary condition in (18) to yield

$$\hat{s}_q(0) = \frac{i}{(q+i0)(1-ivq)(\sqrt{1+q^2-i\alpha vq}-i\beta vq)}. \tag{C.7}$$

Then, applying the inverse Fourier transform

$$s(x, z) = \frac{1}{2\pi} \int_{-\infty}^{+\infty} e^{iqx} \hat{s}_q(z) dq, \tag{C.8}$$

$$p(x) = \frac{1}{2\pi} \int_{-\infty}^{+\infty} e^{iqx} \hat{p}_q dq,$$

we arrive at

$$p(x) = (1 - e^{x/v})H(-x). \tag{C.9}$$

and, in particular,

$$s(0, 0) = \frac{i}{2\pi} \int_{-\infty}^{+\infty} \frac{dq}{(q+i0)(1-ivq)(\sqrt{1+q^2-i\alpha vq}-i\beta vq)}. \tag{C.10}$$

Using contour integration techniques, this integral can be transformed to that given in (25). This is done by observing that the integrand in (C.10) has poles at $q = q_1, q = q_2$ and $q = q_3$, where

$$q_1 = -i0, \quad q_2 = -\frac{i}{v}, \tag{C.11}$$

$$q_3 = \frac{i(\alpha v - \sqrt{\alpha^2 v^2 + 4 + 4\beta^2 v^2})}{2(1 + \beta^2 v^2)},$$

and the branch cut with the required properties can be chosen along the intervals $(-i\infty, q_4)$ and $(q_5, +i\infty)$, where

$$q_4 = \frac{i}{2}(\alpha v - \sqrt{4 + \alpha^2 v^2}), \quad q_5 = \frac{i}{2}(\alpha v + \sqrt{4 + \alpha^2 v^2}), \tag{C.12}$$

along the imaginary axis. Closing the contour of integration by an arc above the real axis and then deforming the contour to lie on the branch cut on the positive imaginary axis, after some algebra we obtain (25).

Without going into too many details, using the same approach, we can also calculate the solution $s(x, z)$ in the extracellular space. The answer can be separated into two parts

$$s(x, z) = \frac{1}{\pi} \int_{\frac{i}{2}(\alpha v + \sqrt{\alpha^2 v^2 + 4})}^{+\infty} \frac{e^{-x\tau}}{\tau(1+v\tau)((1+\beta^2 v^2)\tau^2 - \alpha v\tau - 1)} \times \left[\cos(z\sqrt{\tau^2 - \alpha v\tau - 1})\sqrt{\tau^2 - \alpha v\tau - 1} + v\beta\tau \sin(z\sqrt{\tau^2 - \alpha v\tau - 1}) \right] d\tau, \quad x \geq 0, \tag{C.13}$$

and

$$\begin{aligned}
s(x, z) = & \frac{1}{\pi} \int_{-\infty}^{\frac{1}{2}(\alpha v - \sqrt{\alpha^2 v^2 + 4})} e^{-x\tau} \\
& \times \left\{ \frac{e^{-x\tau}}{\tau(1+v\tau)((1+\beta^2 v^2)\tau^2 - \alpha v\tau - 1)} \right. \\
& \times [\cos(z\sqrt{\tau^2 - \alpha v\tau - 1})\sqrt{\tau^2 - \alpha v\tau - 1} \\
& \left. + v\beta\tau \sin(z\sqrt{\tau^2 - \alpha v\tau - 1}) \right] d\tau \\
& - \frac{2\beta v e^{\frac{(zv\beta - s)(\alpha v - \sqrt{\alpha^2 v^2 + 4\beta^2 v^2 + 4})}{2(\beta^2 v^2 + 1)}}}{\left(1 + \frac{v(\alpha v - \sqrt{\alpha^2 v^2 + 4\beta^2 v^2 + 4})}{2(\beta^2 v^2 + 1)}\right)\sqrt{\alpha^2 v^2 + 4\beta^2 v^2 + 4}} \\
& - \operatorname{Re} \left(\frac{e^{\frac{x}{v} - z\sqrt{1 - \alpha - v^{-2}}} }{\sqrt{1 - \alpha - v^{-2} - \beta}} \right) + e^{-z}, \quad x \leq 0, \quad (\text{C.14})
\end{aligned}$$

where in (C.14) the integral is understood in the sense of Cauchy principal value when the pole at $\tau = -v^{-1}$ lies in the integration segment. As expected, this solution is bounded and has the behavior at infinity given by (20) and (21). Therefore, by the arguments of appendix B it is monotone decreasing in x , consistently with the assumption made at the beginning of the analysis.

Finally, to see that s_T^+ is a monotonically decreasing function of v , α and β , we rewrite the integral in (25) in terms of the new variable ξ , such that

$$\tau = \xi + \xi_0, \quad \xi_0 = \frac{\alpha v + \sqrt{4 + \alpha^2 v^2}}{2}. \quad (\text{C.15})$$

Note that ξ_0 is an increasing function of v and α . Substituting this definition into (25), after some algebra we obtain

$$\begin{aligned}
s_T^+(v) = & \frac{1}{\pi} \int_0^\infty \\
& \times \frac{\sqrt{\xi \left(1 + \frac{1}{\xi_0(\xi + \xi_0)}\right) d\xi}}{\sqrt{\xi + \xi_0(1 + v(\xi + \xi_0))(\beta^2 v^2(\xi + \xi_0)^2 + \xi(\xi + \sqrt{\alpha^2 v^2 + 4}))}}. \quad (\text{C.16})
\end{aligned}$$

From this, by direct inspection it is not difficult to see that the integrand in the above expression is a decreasing function of v , α and β .

Appendix D. Limiting regimes

Here we derive the reduced models in the three asymptotic regimes discussed in section 2.4. In all cases, the model can be reduced to a single integro-differential equation whose properties are similar to that of a scalar reaction-diffusion equation with a bistable nonlinearity.

Case $\alpha \ll 1$ and $\beta \ll 1$. As was already noted, in this case the dynamics of ligands is slaved to that of the intracellular species, and the cell surface capacity is negligible. Setting $\alpha = \beta = 0$ in (9)–(11), we obtain the following reduced problem:

$$\frac{\partial^2 s}{\partial x^2} + \frac{\partial^2 s}{\partial y^2} + \frac{\partial^2 s}{\partial z^2} - s = 0, \quad z > 0, \quad (\text{D.1})$$

$$\frac{\partial s}{\partial z} = -p, \quad z = 0, \quad (\text{D.2})$$

$$\frac{\partial p}{\partial t} = -p + \sigma(s/s_T), \quad z = 0. \quad (\text{D.3})$$

These equations can be further simplified to a single integro-differential equation for the variable $p = p(\mathbf{r}, t)$, where $\mathbf{r} = (x, y)$ is the two-dimensional position vector denoting a point on the epithelium surface. This can be done by explicitly expressing the ligand concentration at the cell surface in terms of the distribution of p , using, e.g., Fourier transform techniques. Omitting the details of this calculation, we arrive at the following effective equation:

$$\frac{\partial p(\mathbf{r}, t)}{\partial t} = -p(\mathbf{r}, t) + \sigma \left(\frac{1}{s_T} \int K(\mathbf{r} - \mathbf{r}') p(\mathbf{r}', t) d\mathbf{r}' \right), \quad (\text{D.4})$$

where the kernel K is given explicitly by

$$K(\mathbf{r}) = \frac{e^{-|\mathbf{r}|}}{2\pi|\mathbf{r}|}. \quad (\text{D.5})$$

We note that this type of models (with non-singular kernels) arises in the studies of phase transitions and networks of coupled neurons (see, e.g. [21, 22]).

Case $\alpha \gg 1$ and $\beta \ll \alpha$. To derive the reduced model in the considered limit, we invoke the quasi steady-state for the dynamics of p and set $\beta = 0$. As a result, we obtain

$$\alpha \frac{\partial s}{\partial t} = \frac{\partial^2 s}{\partial x^2} + \frac{\partial^2 s}{\partial y^2} + \frac{\partial^2 s}{\partial z^2} - s, \quad z > 0, \quad (\text{D.6})$$

$$\frac{\partial s}{\partial z} = -\sigma(s/s_T), \quad z = 0. \quad (\text{D.7})$$

Note that the boundary-value problem above may be written as a single equation in the whole space by an even extension of s to $z < 0$. This results in a single reaction-diffusion equation, with the nonlinearity concentrated at $z = 0$ by a δ -function (see also [18])

$$\alpha \frac{\partial s}{\partial t} = \frac{\partial^2 s}{\partial x^2} + \frac{\partial^2 s}{\partial y^2} + \frac{\partial^2 s}{\partial z^2} - s + 2\sigma(s/s_T)\delta(z), \quad (\text{D.8})$$

The properties of solutions of (D.8) should be closely related to those of the usual scalar reaction-diffusion problems with inhomogeneous sources [12, 14, 15, 17].

Case $\alpha \ll \beta$ and $\beta \gg 1$. To obtain the reduced model, we again use the fact that p is slaved to s and that α can be set to zero in the equation for s . This leads to the following problem:

$$\frac{\partial^2 s}{\partial x^2} + \frac{\partial^2 s}{\partial y^2} + \frac{\partial^2 s}{\partial z^2} - s = 0, \quad z > 0, \quad (\text{D.9})$$

$$\beta \frac{\partial s}{\partial t} = \frac{\partial s}{\partial z} + \sigma(s/s_T), \quad z = 0. \quad (\text{D.10})$$

Once again, solving the boundary-value problem for s in terms of $\bar{s} = s|_{z=0}$ and skipping technical details, we arrive at the following effective integro-differential equation for $\bar{s} = \bar{s}(\mathbf{r}, t)$:

$$\beta \frac{\partial \bar{s}(\mathbf{r}, t)}{\partial t} = \int K(\mathbf{r} - \mathbf{r}') (\Delta_{\mathbf{r}'} - 1) \bar{s}(\mathbf{r}', t) d\mathbf{r}' + \sigma(\bar{s}/s_T), \quad (\text{D.11})$$

where $\mathbf{r} = (x, y)$ denotes a two-dimensional position vector of a point on the epithelium, $\Delta_{\mathbf{r}} = \partial^2/\partial x^2 + \partial^2/\partial y^2$ is the Laplace's operator in the plane, and K is given by (D.5). This equation differs from the more conventional scalar reaction-diffusion equations only by a presence of the convolution term in front of the linear part. Note that similar equations have been studied in the context of nonlocal models of phase transitions (see e.g. [23]).

Appendix E. Numerical method

Our approach to the problem of solving the boundary-value problem for the ligand distribution in the extracellular space uses the concept of optimal grids for approximating the Neumann-to-Dirichlet map for linear elliptic and hyperbolic boundary-value problems [19, 24–28], which is based on the ideas of model reduction methods (see, e.g., [29]). Let us apply the Fourier–Laplace transform to equation (9). As a result, we obtain the following two-point problem:

$$\frac{d^2\hat{s}}{dz^2} = (1 + r + q_1^2 + q_2^2)\hat{s}, \quad \hat{s}|_{z=\infty} = 0, \quad (\text{E.1})$$

where

$$\hat{s} = \int_0^\infty \int_{-\infty}^{+\infty} \int_{-\infty}^{+\infty} e^{-rt - iq_1x - iq_2y} s(x, y, z, t) dx dy dt, \quad (\text{E.2})$$

with boundary data prescribed at $z = 0$. The Neumann-to-Dirichlet map in the transform space reads $\hat{s}(0) = -F(\lambda)\hat{s}'(0)$, where $\lambda = 1 + r + q_1^2 + q_2^2$, the prime denotes differentiation with respect to z , and the impedance function $F(\lambda)$ is $F(\lambda) = 1/\sqrt{\lambda}$.

The next step is to approximate the continuous impedance function $F(\lambda)$ by a discrete one $F_n(\lambda)$ by replacing the second-order derivative in equation (E.1) with a staggered three-point finite difference scheme with n nodes. Then $\hat{s}_0 = -F_n(\lambda)\hat{s}'(0)$, where

$$\hat{v}_{i+1/2} = \frac{\hat{s}_{i+1} - \hat{s}_i}{h_{i+1/2}}, \quad \frac{\hat{v}_{i+1/2} - \hat{v}_{i-1/2}}{h_i} = \lambda\hat{s}_i, \quad i = 0, 1, \dots, n-1, \quad (\text{E.3})$$

$$\hat{v}_{-1/2} = \hat{s}'(0), \quad \hat{v}_{n-1/2} = 0, \quad \hat{s}_n = 0, \quad (\text{E.4})$$

and h_i are the grid steps to be determined. The impedance function for the discrete problem is a rational function which can be written explicitly as a continued fraction [19]

$$F_n(\lambda) = \frac{1}{\lambda h_0 + \frac{1}{h_{1/2} + \frac{1}{\lambda h_1 + \dots + \frac{1}{h_{n-1/2} + \frac{1}{\lambda h_n}}}}}. \quad (\text{E.5})$$

Thus, approximating $F(\lambda)$ by $F_n(\lambda)$ reduces to finding the best rational approximation $\tilde{F}_n(\lambda)$ in the class of rational functions corresponding to the grids with steps $h_i > 0$. To make precise what is meant by the ‘best’ approximation, we

choose to minimize the relative error on a spectral interval to find $\tilde{F}_n(\lambda)$, such that

$$\sup_{\lambda \in [\lambda_{\min}, \lambda_{\max}]} \left| \frac{F(\lambda) - \tilde{F}_n(\lambda)}{F(\lambda)} \right| = \inf_{F_n} \sup_{\lambda \in [\lambda_{\min}, \lambda_{\max}]} \left| \frac{F(\lambda) - F_n(\lambda)}{F(\lambda)} \right|, \quad (\text{E.6})$$

where λ_{\min} and λ_{\max} are the appropriately chosen ‘cutoff frequencies’. As was found by Ingerman, Druskin and Knizhnerman, this variational problem has a unique solution which gives all $h_i > 0$ [19]. Moreover, for n sufficiently large the optimal rational approximant obtained in this way is close to the impedance function of the so-called optimal geometric grid [19]

$$h_0 = \frac{h_{1/2}}{1 + e^{\pi/(2\sqrt{n})}}, \quad h_{i+1/2} = h_{i-1/2} e^{\pi/\sqrt{n}}, \quad (\text{E.7})$$

$$h_i = \sqrt{h_{i+1/2} h_{i-1/2}}.$$

To implement the obtained optimal grid in the original problem, we discretized the problem on a Cartesian product of the usual rectangular grid with step h_\perp in the (x, y) -plane and the optimal grid in the z -direction, in space, and used a simple explicit Euler discretization in time. To accurately resolve the solution, we chose $h_{1/2} = h_\perp$, this choice corresponds to the value of the upper bound λ_{\max} of the spectral interval on which the approximation is optimized to be consistent with the maximum value of λ resolved by the spatial discretization of the Laplacian in the plane. The obtained method is very efficient. For example, we find that only $n = 5$ nodes of the optimal grid is sufficient to get a 2% accuracy. At the same time, the method is very easy to implement.

References

- [1] Martinez-Arias A and Stewart A 2002 *Molecular Principles of Animal Development* (New York: Oxford University Press)
- [2] Shvartsman S Y, Wiley H S, Deen W M and Lauffenburger D A 2001 Spatial range of autocrine signaling: modeling and computational analysis *Biophys. J.* **81** 1854–67
- [3] Nishimura M, Inoue Y and Hayashi S 2007 A wave of EGFR signaling determines cell alignment and intercalation in the *Drosophila* tracheal placode *Development* **134** 4273–82
- [4] Boucher I, Yang L-L, Mayo C, Klepeis V and Trinkaus-Randall V 2007 Injury and nucleotides induce phosphorylation of epidermal growth factor receptor: MMP and HB-EGF dependent pathway *Exp. Eye Res.* **85** 130–41
- [5] Nikolic D L, Boettiger A N, Bar-Sagi D, Carbeck J D and Shvartsman S Y 2006 Role of boundary conditions in an experimental model of epithelial wound healing *Am. J. Physiol. Cell Physiol.* **291** C68–75
- [6] Wesley U V, Bove P F, Hristova M, McCarthy S and van der Vliet A 2007 Airway epithelial cell migration and wound repair by ATP-mediated activation of dual oxidase 1 *J. Biol. Chem.* **282** 3213–20
- [7] Příbyl M, Muratov C B and Shvartsman S Y 2003 Long-range signal transmission in autocrine relays *Biophys. J.* **84** 883–96
- [8] Příbyl M, Muratov C B and Shvartsman S Y 2003 Discrete models of autocrine cell communication in epithelial layers *Biophys. J.* **84** 3624–35

- [9] Muratov C B and Shvartsman S Y 2004 Signal propagation and failure in discrete autocrine relays *Phys. Rev. Lett.* **93** 118101
- [10] Freeman M 2000 Feedback control of intercellular signalling in development *Nature* **408** 313–9
- [11] Huang C Y and Ferrell J E 1996 Ultrasensitivity in the mitogen-activated protein kinase cascade *Proc. Natl Acad. Sci. USA* **93** 10078–83
- [12] Mikhailov A S 1990 *Foundations of Synergetics* (Berlin: Springer)
- [13] Keener J and Sneyd J 1998 *Mathematical Physiology* (New York: Springer)
- [14] Muratov C B and Novaga M 2008 Front propagation in infinite cylinders: I. A variational approach *Commun. Math. Sci.* **6** 799–826
- [15] Xin J 2000 Front propagation in heterogeneous media *SIAM Rev.* **42** 161–230
- [16] Berestycki H and Hamel F 2007 Generalized travelling waves for reaction-diffusion equations *Perspectives in Nonlinear Partial Differential Equations* (Contemp. Math. vol 446) (Providence, RI: American Mathematical Society) pp 101–23
- [17] Fife P C 1979 *Mathematical Aspects of Reacting and Diffusing Systems* (Berlin: Springer)
- [18] Pando B, Pearson J B and Ponce-Dawson S 2003 Sheet excitability and nonlinear wave propagation *Phys. Rev. Lett.* **91** 258101
- [19] Ingerman D, Druskin V and Knizhnerman L 2000 Optimal finite difference grids and rational approximations of the square root: I. Elliptic problems *Commun. Pure Appl. Math.* **53** 1039–66
- [20] Gilbarg D and Trudinger N S 1983 *Elliptic Partial Differential Equations of Second Order* (Berlin: Springer)
- [21] Ermentrout G B and McLeod J B 1993 Existence and uniqueness of traveling waves for a neural network *Proc. R. Soc. Edinb.* **123A** 461–78
- [22] Orlandi E and Triolo L 1997 Travelling fronts in nonlocal models for phase separation in an external field *Proc. R. Soc. Edinb. A* **127** 823–35
- [23] Bates P W, Fife P C, Ren X and Wang X 1997 Traveling waves in a convolution model for phase transitions *Arch. Ration. Mech. Anal.* **138** 105–36
- [24] Druskin V 1997 Spectrally optimal finite difference grids in unbounded domains *Schlumberger-Doll Research Notes* pp EMG–002–97–22
- [25] Asvadurov S, Druskin V and Knizhnerman L 2000 Application of the difference Gaussian rules to solution of hyperbolic problems *J. Comput. Phys.* **158** 116–35
- [26] Asvadurov S, Druskin V and Knizhnerman L 2002 Application of the difference Gaussian rules to solution of hyperbolic problems: II. Global expansion *J. Comput. Phys.* **175** 24–49
- [27] Druskin V and Moskow S 2001 Three-point finite difference schemes, Padé and the spectral Galerkin method: I. One-sided impedance approximation *Math. Comput.* **71** 995–1019
- [28] Posta F, Shvartsman S Y and Muratov C B 2008 Compensated optimal grids for elliptic boundary-value problems *J. Comput. Phys.* **227** 8622–35
- [29] Bai Z 2002 Krylov subspace techniques for reduced-order modeling of large-scale dynamical systems *Appl. Numer. Math.* **43** 9–44